International Journal of Modern Physics C
Vol. 21, No. 6 (2010) 795–811

DOI: 10.1142/S0129183110015488

World Scientific
www.worldscientific.com

UNSTRUCTURED LATTICE BOLTZMANN METHOD FOR HEMODYNAMIC FLOWS WITH SHEAR-DEPENDENT VISCOSITY

J. JANELA

Department of Mathematics-ISEG and CEMAT-IST
1200-781 Lisbon, Portugal
jjanela@iseg.utl.pt

A. SEQUEIRA

Department of Mathematics and CEMAT-IST
1049-001 Lisbon, Portugal
adelia.sequeira@math.ist.utl.pt

G. PONTRELLI* and S. SUCCI†

Istituto per le Applicazioni del Calcolo-CNR
00185 Roma, Italy
**giuseppe.pontrelli@gmail.com*
†*s.succi@iac.cnr.it*

S. UBERTINI

Department of Technology
University of Naples "Parthenope," Napoli, Italy
stefano.ubertini@uniparthenope.it

Received 22 April 2010
Accepted 3 May 2010

The lattice Boltzmann formulation on unstructured grids (ULBE) is compared against semi-analytical solutions of non-Newtonian flows in straight channels, as well as with finite-element simulations in stenosed geometries. In all cases, satisfactory agreement is found, lending further credit to the ULBE method as a potentially useful method for the numerical simulation of small-scale hemodynamic flows, such as blood flow in capillaries and arterioles.

Keywords: Unstructured lattice Boltzmann method; shear-thinning flows; hemodynamics; semi-analytical solution.

*Corresponding author.

1. Introduction

Blood is a concentrated suspension of biological micro/nano bodies, including red blood cells (RBCs or erythrocytes), white blood cells (WBCs or leukocytes) and platelets (thrombocytes). These cellular elements are suspended in a low-viscosity aqueous polymeric and ionic solution, the plasma, containing electrolytes and organic molecules such as metabolites, hormones, enzymes, antibodies and other proteins. These elements are produced in the bone marrow and represent approximately 45% by volume of the normal human blood.[1]

The study of blood flow in the vascular system is complicated in many respects and thus simplifying assumptions are often made.[2] Plasma behaves as a Newtonian fluid, but whole blood exhibits marked non-Newtonian properties, like shear-thinning viscosity, thixotropy, viscoelasticity and possibly a yield stress. This is mostly due to erythrocyte behavior, mainly their ability to aggregate into three-dimensional microstructures (*rouleaux*) at low shear rates, their deformability (or breakup) and their tendency to align with the flow field at high shear rates.[3] In particular, at rest or at low shear rates (below 1 s^{-1}) blood seems to exhibit a high apparent viscosity, while at high shear rates there is a reduction in the blood's viscosity. Attempts to explain the shear-thinning nature of blood were initiated by Chien *et al.*[4] in the 1960s. Empirical models like the power-law, Cross, Carreau or W-S generalized Newtonian fluid models have been obtained, by fitting experimental data in one-dimensional flows.[5,6]

Non-Newtonian homogeneous continuum models are very significant in hemodynamics and hemorheology. However, it should be emphasized that blood flow is Newtonian in most parts of the arterial system and attention should be focused on flow regimes and physiological conditions where non-Newtonian effects are likely to be observed. These include, for normal blood, regions of stable recirculation like in the venous system and parts of the arterial vasculature where geometry has been altered and RBC aggregates become more stable, like downstream at stenosis, inside a saccular aneurysm or in some cerebral anastomoses. In addition, several pathologies are accompanied by significant changes in the mechanical properties of blood and this results in alterations in blood viscosity and viscoelastic properties, as reported in a recent review article.[7]

One of the most frequent abnormalities of the vascular system is the partial occlusion of blood vessels due to stenotic obstruction related to atherosclerosis. There is strong evidence that hemodynamical factors such as flow separation, flow recirculation, low and oscillatory wall shear stress play a major role in the development and progression of atherosclerotic plaques and other arterial lesions,[8] but their specific role is not completely understood. The mathematical and numerical study of meaningful constitutive models, that can accurately capture the rheological response of blood over a range of physiological flow conditions, is recognized as an invaluable tool for the interpretation and analysis of the circulatory system functionality, in both physiological and pathological situations.[9] In the present work

blood is considered as an inelastic shear-thinning fluid modeled by the Carreau non-Newtonian law of viscosity.

Due to the geometrical complexity of the vascular system, even relatively coarse meshes of the regions under analysis can feature millions of elements, leading to very demanding simulations. For this reason, any improvements in the numerical schemes used in flow computations can give access to the solution of problems that were before out-of-reach or enable a faster solution of problems that can nowadays take many hours. In this paper, we will explore the possibility of using an unstructured variant of the lattice Boltzmann method to solve relevant problems in small-scale hemodynamics.

In the last decade lattice Boltzmann (LB) methods have undergone a major progress as an alternative to the discretization of the Navier–Stokes equations for the numerical solution of hemodynamical problems.[10] The standard LB draws much of its conceptual simplicity and computational efficiency from the fact of being formulated in a uniform Cartesian mesh. However, uniform Cartesian grids also represent a severe limitation for many practical engineering and biomedical problems involving real-life complex geometries. Therefore, in the recent years, much research has been directed to the goal of enhancing the geometrical flexibility of the LB method. Indeed, starting from the earliest finite-volume formulations more than a decade ago,[11] today many options are available to deal with realistically complex geometries.[12–14] An interesting development is represented by finite-volume formulations on fully unstructured grids (ULBE).[15] Here the methodology is extended to a more general class of fluids with a shear rate-dependent viscosity, such as the shear-thinning flows.

A preliminary objective of this paper is to validate the fully-developed velocity profile obtained numerically as described in Sec. 3, using benchmark solutions that are available for this simplified problem[16,17] and that will be introduced in Sec. 4. Besides comparisons with analytical solutions, we also present results on an idealized stenosed vessel, and validate ULBE against a finite element solution (Sec. 5).

2. Flow of Shear-Thinning Fluids

We consider the mass and momentum conservation equations for the isothermal flow of an incompressible fluid in a bounded region $\Omega \subset \mathbb{R}^2$:

$$\begin{cases} \rho\left(\dfrac{\partial \mathbf{u}}{\partial t} + \mathbf{u}\cdot\nabla\mathbf{u}\right) = \operatorname{div}\boldsymbol{\sigma}(\mathbf{u},p) & \text{in } \Omega, \forall\ t \in I \\ \operatorname{div}\mathbf{u} = 0 & \text{in } \Omega, \forall\ t \in I \end{cases}, \tag{2.1}$$

where $I = (0,T]$ is the time interval, ρ is the fluid density, and $(\mathbf{u},p)$ are the unknown velocity and pressure. Here $\boldsymbol{\sigma}$ is the Cauchy stress tensor, described through a constitutive relation intended to capture the rheological behavior of blood. In the simplest case, the Newtonian fluid, this constitutive relation is given

by $\boldsymbol{\sigma} = -p\mathbf{I} + \mu(\nabla\mathbf{u} + \nabla\mathbf{u}^T)$, where μ, assumed constant, is the dynamical viscosity of blood.

While this linear relation between stress and strain expressed by the Navier–Stokes equations is acceptable for modeling blood flow in large arteries, at least away from the walls, the rheological behavior of blood, induced by the aggregation and deformability of RBCs, becomes more important at low shear rates ($<100\ \mathrm{s}^{-1}$) or in smaller vessels, where flows cannot be well-described by a simplistic linear constitutive equation.[4]

In the microcirculation, both the Reynolds and Womersley numbers are small because of the small size of the vessels and the low flow velocities. Moreover, near the center of the large vessels, or in separated regions of recirculating flow, the average value of shear rate is generally small. In all these cases, the viscosity cannot be considered as a constant, but must be treated as a decreasing function of the rate of shear $\dot{\gamma}$. In the recent years, many constitutive models have been proposed to capture the material properties blood, in particular models describing the dependence of viscosity on the strain rate.[18] Due to the complex structure of blood and to the variability of flow conditions across the circulatory system, no model seems to be completely satisfactory. Different models must be considered, according to the flow characteristics in the region of interest. Experimental evidence shows that, while the plasma can be considered a Newtonian fluid, when red cells are present the viscosity of the whole mixture increases considerably at low shear rate (*shear-thinning fluid*).[19] Actually, the RBCs tend to aggregate when the shear stress is small and, as a consequence, the apparent viscosity raises. As the shear rate increases, the aggregates are broken and red blood cells become individualized, resulting in a decrease of the apparent viscosity. At very high shear rates, the stresses are sufficient to deform the cells extensively, aligning with the main flow and reducing the dissipation of energy, which results in a further decrease of the viscosity.

From the modeling point of view, the shear-thinning viscosity of blood is introduced through a constitutive relation where viscosity depends on shear rate $\dot{\gamma}$, more precisely, the Cauchy stress tensor is given by $\boldsymbol{\sigma} = -p\mathbf{I} + \mu(\dot{\gamma})(\nabla\mathbf{u} + \nabla\mathbf{u}^T)$. The viscosity function $\mu(\cdot)$ is prescribed *a priori* by curve fitting from experimental data. Many viscosity models were proposed in the literature[7] but, as long as they provide a good fit to experimental viscosity data, there is no reason to prefer one over the other. These models generally take the form

$$\mu(\dot{\gamma}) = \mu_\infty + (\mu_0 - \mu_\infty)F(\dot{\gamma})\,,$$

where μ_0 and μ_∞ are the asymptotic viscosities at zero and infinity shear rates, and $F(\dot{\gamma})$ is a smooth function making the transition between the asymptotic viscosities. In this study, we use the Carreau model[9] given by

$$\mu(\dot{\gamma}) = \mu_\infty + (\mu_0 - \mu_\infty)(1 + (\lambda\dot{\gamma})^2)^{(n-1)/2}\,. \tag{2.2}$$

As mentioned before, the parameters are estimated from experimental data, using a nonlinear least-squares technique. The most sensitive parameters are μ_0

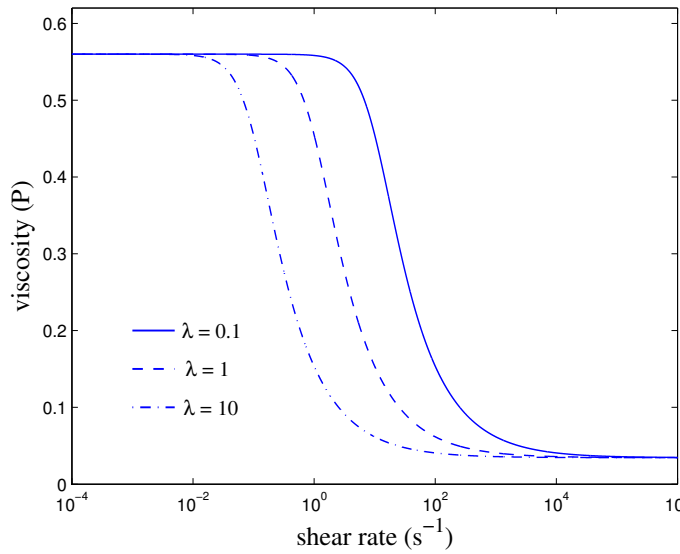

Fig. 1. The shear-thinning viscosity curves for three values of λ.

and λ. They are in fact extrapolated from data because of technical difficulties in measuring viscosity at low shear rates (less than 1 s^{-1}). The parameter λ, with dimensions of time (sometimes abusively referred to as a relaxation time), controls the transition region where the viscosity drop occurs and can significantly affect the numerical results (see Fig. 1). It is found that λ varies considerably with the population datasets (gender, age, race, etc. . . .) and small errors in blood viscosity measurements can affect its numerical value. In the following, we will use a basic set of parameters taken from Ref. 20 and analyze the sensitivity of the model to variations of the parameter λ.

3. The Lattice Boltzmann Equation on Unstructured Grids

The lattice Boltzmann method (LBM) has become an established numerical approach in computational fluid dynamics for solving a wide range of complex fluids and flows, including non-Newtonian and blood flows.[21] The LBM is based on a minimal kinetic Boltzmann equation in which representative particles evolve on a regular Cartesian grid according to simple streaming and collision rules, designed in such a way as to preserve the conservation laws of fluid dynamics. This method features a number of advantages over conventional CFD methods, i.e. simplicity, amenability to parallel computing, ease in handling complex flows, but the use of constant particle speeds in space necessarily imposes a spatially uniform Cartesian grid. This represents a severe limitation for many practical applications, particularly for complex geometries where a selective distribution of the computational degrees of freedom in the "hot" regions is necessary. Among the various options to enhance geometrical flexibility,[10,13] an interesting one is represented by the finite

volume formulation on unstructured grids.[11,15,22] The Unstructured Lattice Boltzmann Scheme (ULBE for short) solves the differential form of the lattice Boltzmann equation:

$$\partial_t f_i + \mathbf{c}_i \cdot \nabla f_i = -\frac{(f_i - f_i^{\mathrm{eq}})}{\tau} \tag{3.1}$$

where the velocity-space is discretized into a finite number of particle states i. The variable $f_i(\mathbf{x}, t) \equiv f(\mathbf{x}, \mathbf{v} = \mathbf{c}_i, t)$ (density distribution function or population) is the probability of finding a particle at site $\mathbf{x}$, at time t and moving along the lattice direction defined by the discrete speed $\mathbf{c}_i$. The right-hand side of the above equation is the Bhatnagar–Gross–Krook (BGK) collision operator, which represents particle interactions via a single-time relaxation towards local equilibrium f_i^{eq} on a single timescale τ. This relaxation timescale fixes the kinematic viscosity of the LB fluid, according to $\nu = c_s^2(\tau - \Delta t/2)$. The local equilibrium distribution is given by the Maxwell–Boltzmann distribution expanded in Taylor series of the fluid speed up to second-order:

$$f_i^{\mathrm{eq}} = \rho w_i \left[1 + \beta u_i + \frac{1}{2}(\beta^2 u_i^2 - \beta u^2)\right] \tag{3.2}$$

where $u_i = \mathbf{u} \cdot \mathbf{c}_i$, $\beta = 1/c_s^2$, c_s being the lattice sound speed, ρ the fluid density, $\mathbf{u}$ the fluid speed and w_i the associated weight coefficients. Through a Chapman–Enskog analysis, the LBM is proved to reproduce the Navier–Stokes equations near the incompressibility limit. The fluid macroscopic variables are calculated as mass density $\rho = \sum_i f_i$, velocity $\mathbf{u} = \sum_i \mathbf{c}_i f_i/\rho$ and pressure $p = \rho c_s^2$. In order to recover the correct fluid dynamic equations in the macroscopic limit, the discretization of the velocity space must be performed in such a way as to conserve mass and momentum, as well as rotational symmetry. In this work, the two-dimensional nine-speed model (known as D2Q9) is used[23]:

$$\begin{aligned}
&\mathbf{c}_0 = (0,0)\,, \quad && \mathbf{c}_1 = (1,0)\,, && \mathbf{c}_2 = (0,1)\,,\\
&\mathbf{c}_3 = (-1,0)\,, && \mathbf{c}_4 = (0,-1)\,, && \mathbf{c}_5 = (1,1)\,,\\
&\mathbf{c}_6 = (-1,1)\,, && \mathbf{c}_7 = (-1,-1)\,, && \mathbf{c}_8 = (1,-1)\,,
\end{aligned}$$

with weights $w_0 = 4/9$, $w_{1-4} = 1/9$, $w_{5-8} = 1/36$ in Eq. (3.2). In the ULBE approach, the lattice Boltzmann equation within BGK approximation is solved by means of a cell-vertex finite-volume scheme applied to fully unstructured grids. The computational domain is subdivided into control volumes of polygonal shape, that permit to adapt the local grid resolution to boundaries of virtually arbitrary shape.

The nine discrete populations $f_i(\mathbf{x}, t)$ associated with each node P of the discrete grid (Fig. 2) represent the unknowns of the problem. The finite volume over which Eq. (3.1) is integrated, is defined by means of the set of K triangles sharing P as a common vertex. Since the discrete grid is unstructured, each node is identified by its coordinates and the connectivity (P, P_k, $P_k + 1$ in Fig. 2) is free to change from node to node. As shown in Fig. 2, the portion of the control volume $[C_k, E_k, P, E_{k+1}]$

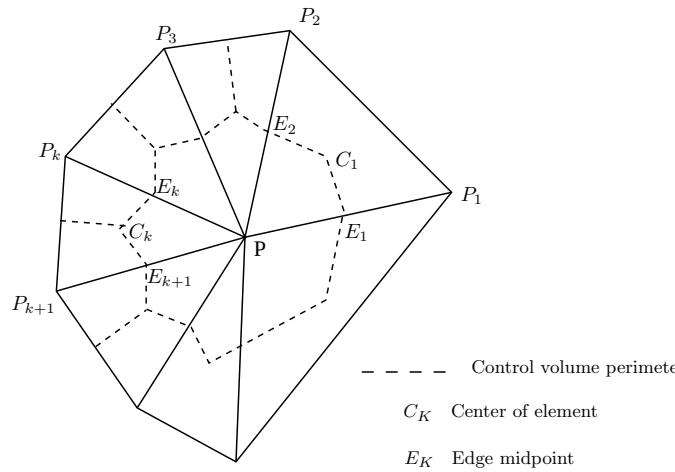

Fig. 2. The cell-vertex finite volume discretization around a grid point P.

that refers to the kth triangular element is built through the union of the two sub-grid triangles $\Omega_k^- = [P, E_k, C_k]$ and $\Omega_k^+ = [P, C_k, E_{k+1}]$, where C_k is the center of the grid element and E_k and E_{k+1} are the midpoints of the edges that share P as a common vertex. Populations at off-grid points E_k and C_k are calculated through standard linear interpolations. Application of the Gauss theorem to each finite volume portion, yields the following set of ordinary differential equations:

$$\partial_t f_i(P,t) = \frac{1}{\Omega_P} \sum_k (\Phi_{ik} - \Xi_{ik}) \tag{3.3}$$

where the sum $k = 0,\ K$ runs over the control volume $\Omega_P = \cup_k \Omega_k$ obtained by joining the centers C_k with edge midpoints E_k. Finally, Φ_{ik} denote the fluxes associated with streaming operator and Ξ_{ik} the integral of the collision operators of the ith population at the kth node, respectively.[22] The detailed expressions of the streaming and collision matrices S_{ik} and $C_{ik} = C_k \delta_{ik}$, give the following fundamental system update equation:

$$\partial_t f_i(P,t) = \sum_{k=0}^{K} S_{ik} f_i(P_k,t) - \frac{1}{\tau} \sum_{k=0}^{K} C_{ik} [f_i(P_k,t) - f_i^{\mathrm{eq}}(P_k,t)]\,. \tag{3.4}$$

By definition the following sum rules come out:

$$\sum_{k=0}^{K} S_{ik} = 0\,, \quad \sum_{k=0}^{K} C_{ik} = 1\,, \quad \forall\ i\,.$$

The method has been found to yield the following viscosity:

$$\nu = c_s^2 \tau$$

in contrast with standard LB, which features:

$$\nu = c_s^2 \left(\tau - \frac{\Delta t}{2} \right) .$$

As pointed out in Ref. 15, the shift $-\Delta t/2$ has far-reaching consequences for the computational efficiency of high-Reynolds flow simulations. For a NN fluid the viscosity changes in function of the strain tensor. This means that for the ULBE simulation the relaxation parameter is changed according to:

$$\tau(t) = \frac{\nu(t)}{c_s^2} . \tag{3.5}$$

The particle distribution functions at the boundaries are calculated by adding the edge-streaming fluxes and imposing the macroscopic condition (i.e. $u = 0$ for no slip) when computing the equilibrium distribution. The edge fluxes are explicitly evaluated by using linear interpolation at the boundary edges. This boundary treatment is called covolume method and works for the generic boundary geometries supporting relatively strong boundary gradients. The use of regular buffers at inlet/outlet sections was found to improve the stability of ULBE computations for open flows.

3.1. *Extension to NN flows and scaling*

A useful property of the LBM is that the strain and the stress tensors are locally available from second-order moments of the (non-equilibrium) distribution functions:

$$\mathbf{\Gamma}_{\alpha\beta} = -\frac{1}{2\rho\tau c_s^2} \mathbf{\Pi}_{\alpha\beta} \tag{3.6}$$

where

$$\mathbf{\Pi}_{\alpha\beta} = \sum_i (f_i - f_i^{\mathrm{eq}}) \mathbf{c}_{i\alpha} \mathbf{c}_{i\beta} \tag{3.7}$$

and α, β run over spatial dimensions. However, this property is spoiled by standard LBE, because the body surface does not generally lie on lattice sites (staircase effects), so that interpolations are required to calculate the aerodynamic force. This advantage is instead fully realized by ULBE, since nodal unknowns can be placed exactly on the body surface. By calculating the norm of the previous tensors as follows:

$$\dot\gamma \equiv 2|\mathbf{\Gamma}| = 2 \sqrt{\sum_{\alpha,\beta} \Gamma_{\alpha\beta}\Gamma_{\alpha\beta}} , \quad \sigma \equiv |\mathbf{\Pi}| = \sqrt{\sum_{\alpha,\beta} \Pi_{\alpha\beta}\Pi_{\alpha\beta}} \tag{3.8}$$

the strain-stress relation results into the following expression:

$$\dot\gamma = \frac{\sigma}{\rho\tau(\dot\gamma)c_s^2} \tag{3.9}$$

and, being $\mu(\dot\gamma) = \rho\nu(\dot\gamma)$, from Eq. (3.5) we have:

$$\sigma = \mu(\dot\gamma)\dot\gamma . \tag{3.10}$$

In principle $\dot{\gamma}$ can be obtained by solving the above nonlinear Eq. (3.10) by iteration at each lattice site. However, due to the slow variation of $\mu(\dot{\gamma})\dot{\gamma}$ on a timescale Δt, current practice shows that one can adjust τ along the time integration as follows:

$$\tau(t + \Delta t) = \frac{\mu[\dot{\gamma}(t), t]}{\rho(t) c_s^2} \,. \tag{3.11}$$

Note that Eq. (3.10) yields the standard scalar relation $\sigma = \mu\dot{\gamma}$ in the Newtonian case.

The LB (overbarred) variables are defined as scaled quantities such that their combination matches the physical Reynolds number as:

$$\frac{\rho U_{\max}(2H)}{\mu_0} = \mathrm{Re}_{\mathrm{phys}} = \mathrm{Re}_{\mathrm{LB}} = \frac{\bar{\rho}\bar{U}_{\max}(2\bar{H})}{\bar{\mu}_0}$$

whence:

$$\beta = \frac{\bar{\mu}_0}{\mu_0} = \frac{\bar{\mu}_\infty}{\mu_\infty} = \frac{\bar{\rho}\bar{U}_{\max}\bar{H}}{\rho U_{\max} H} \,. \tag{3.12}$$

β is an input parameter that fixes the two limiting LB viscosities and determines the scaling of LB problem. Physical variables are related to the corresponding LB variables by:

$$u = \frac{\bar{\rho}\bar{H}}{\beta\rho H}\bar{u} \qquad \lambda = \frac{\beta\rho H^2}{\bar{\rho}\bar{H}^2}\bar{\lambda} \qquad \sigma = \frac{\bar{\rho}\bar{H}^2}{\beta^2\rho H^2}\bar{\sigma}$$

and similarly for the other variables.

4. Validation of ULBE Simulations for Shear-Thinning Flows

In idealized geometries and under particular flow conditions, it is possible to obtain closed form solutions for some flow problems, such as the well-known Poiseuille solution for Newtonian flows in a straight pipe.

4.1. *Semi-analytical solutions*

In order to validate the ULBE technique, we compare it against semi-analytical solutions, recently introduced by Janela and Sequeira[16] and later developed in Ref. 17.

Under the specific geometry and flow conditions depicted in Fig. 3, the flow equations simplify considerably. Searching for solutions with the velocity field of the form $\mathbf{u} = (u(y), 0)^T$, yields

$$\boldsymbol{\tau} = \mu(\dot{\gamma}) \begin{pmatrix} 0 & \dot{\gamma} \\ \dot{\gamma} & 0 \end{pmatrix} \,, \quad \nabla p = (G, 0)^T \,,$$

where $\dot{\gamma} = u'(y)$ and $\boldsymbol{\sigma} = -p\mathbf{I} + \boldsymbol{\tau}$. In this case the continuity equation is automatically satisfied and the momentum equations reduce to:

$$\frac{\partial \tau_{11}}{\partial x} + \frac{\partial \tau_{12}}{\partial y} = \frac{\partial p}{\partial x} \Leftrightarrow \frac{d}{dy}\left(\mu\left(\left|\frac{du}{dy}\right|\right)\frac{du}{dy}\right) = G \,. \tag{4.1}$$

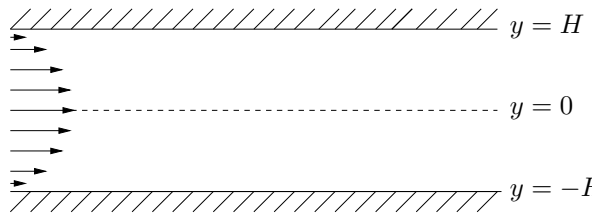

Fig. 3. 2D flow straight channel geometry.

Assuming regularity and boundedness of the stress tensor, the previous equation can be integrated explicitly, to yield:

$$\mu(|\dot{\gamma}|)\dot{\gamma} = Gy\,. \tag{4.2}$$

Since $\dot{\gamma}$ appears in the viscosity function, Eq. (4.2) is in fact a differential equation in the implicit form and must therefore be solved by an iterative procedure. More precisely, $\dot{\gamma}(y)$ is computed from the following fixed point iteration:

$$\begin{cases} \dot{\gamma}^{(0)} \\ \dot{\gamma}^{(n+1)} = \dfrac{Gy}{\mu(\dot{\gamma}^{(n)})} \end{cases} . \tag{4.3}$$

The convergence of this algorithm depends only on the pressure gradient and on the properties of the viscosity function. Having in mind the Carreau viscosity law (2.2), we focus on a class of viscosity functions which are bounded and decreasing in $[0, +\infty)$. The following results are obtained for the Carreau model, but are in fact more general.

Proposition 1. (Global convergence) *If* $|\mu'| \leq \mu_\infty^2/(y|G|)$ *then, for every* $\dot{\gamma}^{(0)} \in [-Gy/\mu_\infty, Gy/\mu_\infty]$, *the fixed point iteration defined by* (4.3) *converges.*

This sufficient condition for global convergence is too strong in many practical cases (for instance in non-Newtonian blood flow simulations the parameter μ_∞ is of the order of 10^{-3}) and also seems to indicate that convergence is more likely to occur for small values of y, which is not the case observed numerically. As a result, we shall derive a local convergence result that is valid over a wide range of parameters.

Proposition 2. (Local convergence) *Suppose that the initial approximation is sufficiently close to the fixed point. Then, if* $|n - 1| < 1$, *the fixed point iteration defined by* (4.3) *converges linearly.*

After computing $\dot{\gamma}$, the velocity profile can be recovered by any suitable adaptive numerical quadrature using the formula

$$u(y) = \int_{-H}^{y} \dot{\gamma}(s)ds\,. \tag{4.4}$$

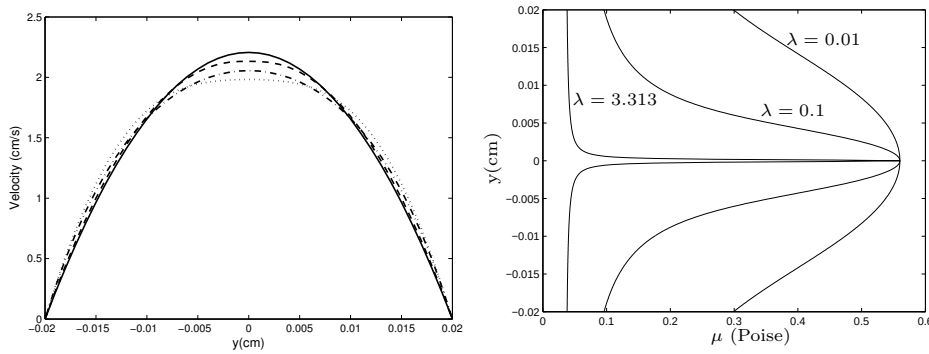

(a) (b)

Fig. 4. (a) Three velocity profiles in a cross-section in the non-Newtonian case, with $\lambda = 0.01$, 0.1, 3.313 s (dash-dotted, dotted and dashed lines, respectively) and the corresponding Newtonian case ($\lambda = 0$, continuous line). Due to a larger value of the viscosity at low shear rates, the profile flattens in the core region. (b) The shear rate viscosity profiles along the cross-section for the same values of λ.

We observe that the primitive variable is in fact the stress, and that the velocity is obtained by post-processing. Also the wall shear rate $\dot{\gamma}_w$ and the wall shear stress $\sigma_w = \mu(\dot{\gamma}_w)\dot{\gamma}_w$ can be computed directly as primitive variables. In Fig. 4, we exhibit the velocity and viscosity profiles corresponding to the set of parameters, computed to a prescribed precision of 10^{-12}, to be used to benchmark the ULBE solutions introduced in the next subsection.

4.2. *Benchmarking of ULBE simulations*

The method described in the previous subsection provides benchmark solutions to the simplified problem outlined in Fig. 3. A parabolic velocity profile with maximum velocity $U_{\max}$ is imposed at the inflow section and a zero traction condition is imposed at the outlet. Being the fluid non-Newtonian, a finite entry length must be covered before the flow becomes fully developed. To this aim, we consider a channel of length L with a sufficiently high L/H ratio. The chosen geometry and flow conditions are compatible with blood flow in an arteriole or small artery, namely

$$\begin{aligned} &\rho = 1 \text{ g/cm}^3 \qquad U_{\max} = 2.2 \text{ cm/s} \qquad H = 0.02 \text{ cm} \\ &\mu_0 = 0.56 \text{ Poise} \qquad \mu_0 = 0.0345 \text{ Poise} \end{aligned} \tag{4.5}$$

giving rise to $\text{Re}_0 = 0.157$. The value of λ is set to vary around a physiological range.[1]

A set of ULBE simulations has been carried out with the parameters in Eq. (4.5). The computational domain has been normalized to the rectangle $[-3, 3] \times [-1, 1]$, covered by a grid consisting of 4149 uniformly distributed nodes (with 27 nodes at inlet and outlet), 8094 triangular elements, $\Delta t = 0.005$, $\bar{\rho} = 1$, $\beta = 0.05$ to cover a wide range of LB admissible viscosities (see Eq. (3.12)). To assess the grid

resolution, the first simulation concerns the case of the Newtonian flow ($\mu = \mu_0$ or $\mu = \mu_\infty$): comparison of the ULBE solution with the Poiseuille velocity profile

$$u(y) = U_{\max}\left(1 - \frac{y^2}{H^2}\right) \tag{4.6}$$

gives a maximum error $E \simeq 10^{-5}$, whereas the discrepancy with the wall shear rate and stress:

$$\dot{\gamma} = \frac{2U_{\max}}{H} \quad \text{and} \quad \sigma = \frac{2\mu U_{\max}}{H} \tag{4.7}$$

results in $E \simeq 10^{-4}$ (see Ref. 21).

In the non-Newtonian case, for $\lambda = 3.31$ s, the velocity $U_{\max}$ drops to a lower value and the profile flattens, with respect to the Newtonian case, due to the viscosity rise towards the channel's centerline [see Fig. 4(a)].

To study additional flow regimes, the value of λ was varied over a wide range: the solution goes from a Newtonian regime (λ small) with higher viscosity μ_0 (for all the shear rates experienced during the flow) to another Newtonian regime (λ large) with a lower μ_∞, almost everywhere except near the center where $\dot{\gamma} \to 0$ and μ raises up to $\lim_{y\to 0} \mu(r) = \mu_0$ in Fig. 1. Because we are imposing a parabolic profile at the inflow section, these limiting solutions yield the same velocity profile, if only with different viscosity and pressure gradient. It is worth noting that LB methods work properly only within a limited range of the kinematic viscosity $\bar{\nu}$ (in lattice units), typically range $1/N < \bar{\nu} < 1$, N being the number of grid points per linear dimension. Values below the lower bound may trigger numerical instabilities in the presence of sharp gradients, due to insufficient small-scale dissipation. Values above the upper bound, on the other hand, undermine the adiabatic assumption, i.e. fast enslaving of the stress tensor to its equilibrium value, which lies behind the hydrodynamic limit of the LB equation.

In the transition shear-thinning region, the solution changes qualitatively, the shear-dependent viscosity rises in the core region where the shear is low, and the parabolic shape appears flattened in the center of the channel. It turns out that λ plays a critical role since its values influences the local viscosity in Fig. 1. Tables 1–2,

Table 1. Values of $U_{\max}$, effective μ_∞ (viscosity at the wall) and WSS for several values of λ ($n = 0.3568$). The last two columns display the relative errors with the semi-analytical solution.

λ	$U_{\max}$	μ_{wall}	WSS	G	%Err. $U_{\max}$	%Err. WSS
0	2.20	0.56	122.5	6179	0.31	0.87
0.01	2.06	0.29	80.82	4080.5	−0.24	0.96
0.1	1.97	0.09	26.5	1348.5	0.58	1.70
1	2.07	0.04	11.98	605	0.79	1.48
3.31	2.12	0.04	9.6	486	0.57	1.23
10	2.16	0.038	8.55	432	0.08	1.04

Table 2. Values of $U_{\max}$, effective μ_∞ (viscosity at the wall) and WSS for several values of n ($\lambda = 3.31$). The last two columns display the relative errors with the semi-analytical solution.

n	$U_{\max}$	μ_∞	WSS	G	%Err. $U_{\max}$	%Err. WSS
1	2.20	0.56	122.3	6177	0.27	1.00
0.8	2.13	0.17	40.10	2025	−0.13	0.99
0.6	2.09	0.07	16.84	853	0.55	1.29
0.3568	2.12	0.04	9.6	486	0.57	1.23
0.1	2.17	0.035	7.96	390.2	−3.15	−2.00
0	2.18	0.035	7.76	394	0.60	2.16

show for different values of n and λ, the following quantities: maximum velocity in the fully developed flow region ($U_{\max}$); viscosity at the wall (μ_{wall}); and wall shear stress in the fully developed flow region (WSS). The value of the pressure gradient G is obtained from the ULBE numerical simulations and is needed to construct the semi-analytical solution. As we can see from Tables 1–2, the ULBE results show a satisfactory agreement with the semi-analytical solutions in all cases.

5. Flow Through a Stenosed Channel

Next, let us consider a rectangular channel of longitudinal extension $[-L, L]$ with flat walls everywhere, except for a smooth contraction in a small region centered at $x = 0$. This contraction (stenosis) is described by the following analytic function:

$$\frac{H(x)}{H_0} = 1 - \delta e^{-\phi(x/H_0)^2} \tag{5.1}$$

where $H(x)$ is the height, $0 \leq \delta < 1$ is a measure of the degree of constriction, ϕ of its length in Fig. 5. The value of ϕ should be taken sufficiently small to guarantee a slowly varying boundary profile. The flat rectangular channel is recovered in the limit $\delta \to 0$. The main numerical parameters of the simulation are:

$$L = 0.1 \text{ cm} \qquad H_0 = 0.02 \text{ cm} \qquad \phi = 0.8 \qquad \delta = 0.3$$

corresponding to a degree of contraction of about 50%, for a circular cross-section pipe.[24]

The pressure gradient, the rheological parameters and LB settings are the same as in the straight channel flow ($\lambda = 0.15$ s, $n = 0.3568$).

It has been shown that ULBE offers the possibility to concentrate the number of nodes in the critical regions only, keeping the overall number of degrees of freedom relatively low.[21] In the following simulations, a nonuniform mesh having 3648 nodes and 7010 elements, refined near the contraction, has been chosen in Fig. 5.

In the present Carreau model, the limiting values for viscosities are $\mu_0 = 0.56$ Poise, $\mu_\infty = 0.0345$ Poise (LB units: $\bar{\mu}_0 = 0.028$, $\bar{\mu}_\infty = 1.725 \cdot 10^{-3}$), and the local viscosity in all simulations is found to remain above the lower bound $\mu_{\min} = 0.062$ Poise (LB units $\bar{\mu}_{\min} = 3.10 \cdot 10^{-3}$). The viscosity contour lines for the

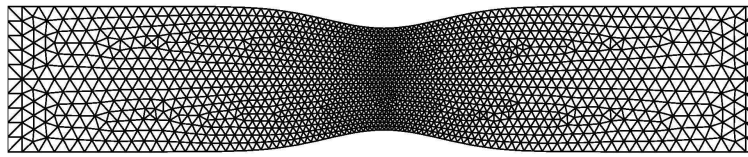

Fig. 5. The axisymmetric stenosed rectangular channel defined by Eq. (5.1) covered by a triangular mesh (3648 nodes and 7010 elements) refined in the contraction area. Several layers of regular elements are added at inlet and outlet.

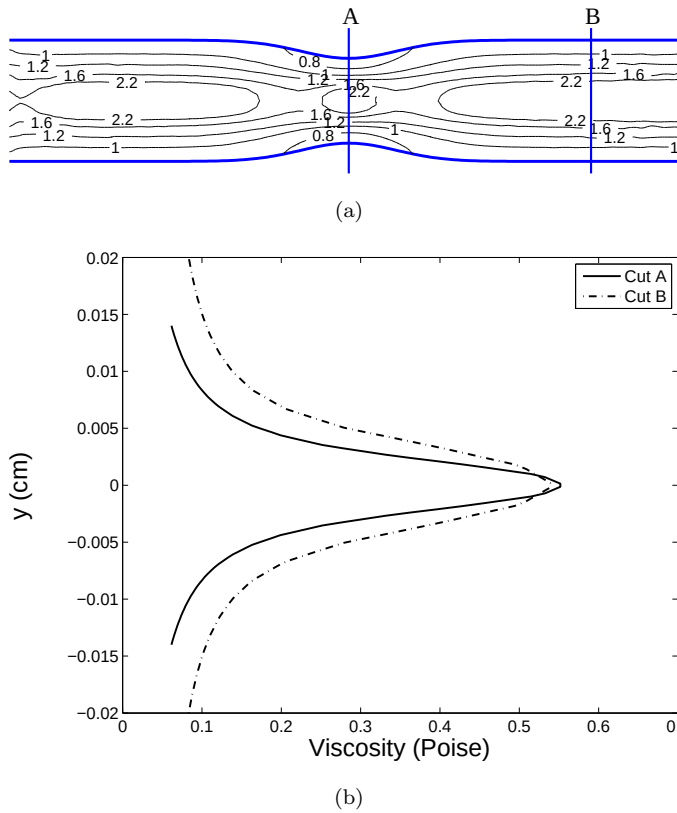

Fig. 6. (a) Viscosity (values $*10$) contour lines, and (b) profiles across sections A and B for the Carreau model Eq. (2.2).

Carreau model are depicted in Fig. 6. For $\lambda > 1$, the viscosity exhibits a pronounced peak along the midline. The velocity profiles are of interest, since they provide a detailed description of the flow field. At that low Reynolds number and for such a mild contraction, neither recirculation, nor flow reversal are observed and the flow appears to be symmetric upstream and downstream the stenosis. The magnitude of the velocity is larger in the Newtonian case in Fig. 7. In the presence of a narrowing, the flow exhibits additional resistance, hence an enhanced shear stress.

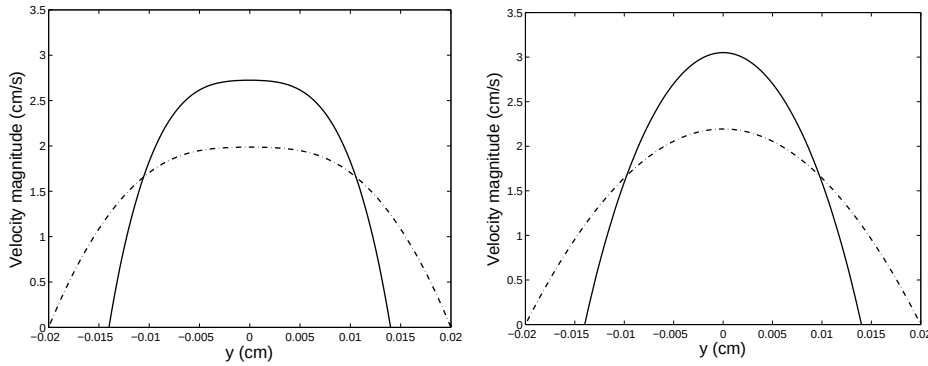

(a) (b)

Fig. 7. Velocity profiles in the throat (continuous) and few diameters downstream (dashed). Plots compare the Carreau model $\mu_0 = 0.56$, $\mu_\infty = 0.0345$, $\lambda = 0.15$ (a) to the Newtonian case $\mu = 0.0345$ (b).

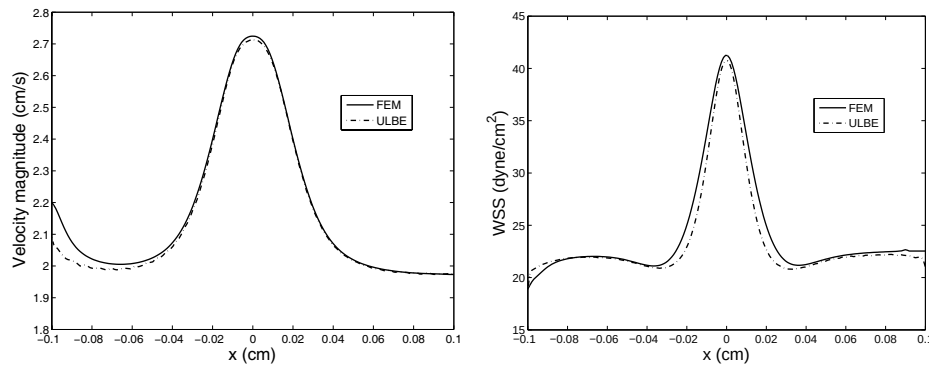

(a) (b)

Fig. 8. (a) Velocity magnitude at the vessel centerline computed with the FEM (solid line) and the ULBE (dashed line) methods. (b) Wall shear stress along the top wall computed with the FEM (solid line) and the ULBE (dashed line) methods.

These indicators of flow disturbances bear significant physiological relevance. Since there is no reliable method of determining the wall shear stress experimentally near the regions of possible reversal flow, numerical experiments represent a valuable (non-invasive) tool, because they offer a sufficiently accurate approximation of the flow configuration. The wall shear stress increases smoothly in correspondence of the contraction and shows a peak value placed symmetrically at the center of the throat. Downstream, it goes back to the previous value. The wall shear stress is higher in NN case, because of the higher shear rate and the higher lower bound viscosity in Fig. 8. All these results are in qualitative agreement with those obtained by other models in literature.[25]

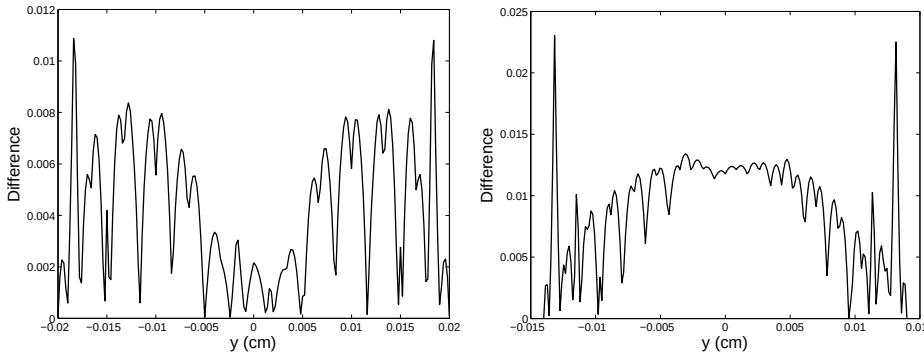

(a) (b)

Fig. 9. Difference between the velocity profiles computed by FEM and ULBE in the throat (a) and a few diameters downstream (b). The maximum difference is in both cases less than 0.02 and halved in the finer grid region.

Since for this geometry there is no closed form or semi-analytical reference solution, as a further validation test, we compared ULBE against finite element solutions over the same grid for several flow cases. The comparisons are displayed in Fig. 9 and show satisfactory agreement between the two methods, with a relative discrepancy of a few percent.

6. Conclusions

Summarizing, we have presented an extension of the lattice Boltzmann method on unstructured grids to the case of non-Newtonian flows, with specific focus on two-dimensional blood flow problems. This extension has been validated against a recent class of analytical solutions for simple geometries, as well as with finite-element solutions for the case of stenosed channels. In all cases, satisfactory agreement is found, lending credit to the ULBE methods as a potential new entry in the list of numerical methods for non-Newtonian flows. Much work remains to be done for the future. Among others, the extension to three-dimensional geometries appears as one of the most compelling issues in order to put ULBE on a firm basis for the simulation of complex hemodynamical flows.

Acknowledgments

The work has been developed and partially funded within the CNR-FCT bilateral project: *Multiscale analysis and numerical simulation of mathematical models in hemodynamics and hemorheology* (2009–2010). The CNR Italian project "Bioinformatics" is also kindly acknowledged.

References

1. C. G. Caro, T. J. Pedley, R. C. Schroter and W. A. Seed, *The Mechanics of the Circulation* (Oxford Univ. Press, Oxford, 1978).
2. L. Formaggia, A. Quarteroni and A. Veneziani (eds.), *Cardiovascular Mathematics: Modeling and Simulation of the Circulatory System*, Series: MS&A, Vol. 1 (Springer, Berlin, 2009).
3. S. Chien, S. Usami, R. J. Dellenback and M. I. Gregersen, *Am. J. Physiol.* **219**, 136 (1970).
4. S. Chien, S. Usami, R. J. Dellenback and M. I. Gregersen, *Science* **157**, 829 (1967).
5. F. J. Walburn and D. J. Schneck, *Biorheology* **13**, 201 (1976).
6. B. R. Bird, R. C. Armstrong and O. Hassager, *Dynamics of Polymeric Liquids* (John Wiley and Sons, New Jersey, 1987).
7. A. M. Robertson, A. Sequeira and M. V. Kameneva, *Hemorheology, Hemodynamical Flows: Modeling, Analysis and Simulation*, Oberwolfach Seminars, Vol. 37, eds. G. P. Galdi, R. Rannacher, A. M. Robertson and S. Turek (Birkhäuser Verlag, 2008), pp. 63–120.
8. S. A. Berger and L. D. Jou, *Ann. Rev. Fluid Mech.* **32**, 347 (2000).
9. D. O. Lowe, *Clinical Blood Rheology* (CRC Press, USA, 1998).
10. R. Ouared and B. Chopard, *J. Stat. Phys.* **121**, 209 (2005).
11. G. Peng, H. Xi and C. Duncan, *Phys. Rev. E* **58**, R4124 (1998).
12. A. Artoli, A. Sequeira and J. Janela, *J. Biomech.* **39**, 310 (2006).
13. M. Bernaschi, S. Melchionna and S. Succi, *Comp. Phys. Comm.* **180**, 1495 (2009).
14. S. Melchionna, M. Bernaschi and S. Succi, *Comp. Phys. Comm.* **181**, 462 (2010).
15. S. Ubertini, G. Bella and S. Succi, *Phys. Rev. E* **68**, 016701 (2003).
16. J. Janela and A. Sequeira, *Proc. Conf. on Topical Problems in Fluid Mech.*, 28 February–2 March, 2007, Prague, Czech Republic.
17. J. Janela, A. Sequeira and A. Moura, *Advances in Mathematical Fluid Mechanics* (Springer, Berlin, 2010), pp. 303–319.
18. S. Chien, S. Usami, H. M. Taylor, J. L. Lundberg and M. I. Gregersen, *J. Appl. Physiol.* **21**, 81 (1966).
19. A. Sequeira and J. Janela, *Proc. Appl. Math. Mech.* **7**, 1101207 (2007).
20. Y. I. Cho and K. R. Kensey, *Biorheology* **28**, 241 (1991).
21. G. Pontrelli, S. Ubertini and S. Succi, *J. Stat. Mech: Theor. Exp.* P06005 (2009).
22. S. Ubertini and S. Succi, *Progr. Comput. Fluid Dynamics* **5-1/2**, 84 (2005).
23. R. Benzi, S. Succi and M. A. Vergassola, *Phys. Rep.* **222**, 145 (1992).
24. G. Pontrelli, *Proc. Inst. Mech. Eng. H.* **215**, 1 (2001).
25. J. Boyd, J. M. Buick and S. Green, *Phys. Fluids* **19**, 093103 (2007).